minerals

MDPI

Article

Petrogenesis of Heavy Rare Earth Element Enriched Rhyolite: Source and Magmatic Evolution of the Round Top Laccolith, Trans-Pecos, Texas

Brent A. Elliott

The Bureau of Economic Geology, The University of Texas at Austin, Austin, TX 78712, USA; brent.elliott@beg.utexas.edu; Tel.: +1-512-471-1812

Received: 9 August 2018; Accepted: 17 September 2018; Published: 22 September 2018

Abstract: The Round Top rhyolite located in Trans-Pecos Texas is enriched in Be, F, Li, Nb, Rb, Sn, Th, U, Y, Zr, and rare earth elements (REEs). REE-bearing minerals are mainly ubiquitous nano-scale accessory phases throughout the groundmass, incorporated in synchysite-group minerals, xenotime-(Y), Y- and Ce-rich fluorite, and zircon. The rhyolite is peraluminous, high-silica, alkaline (not peralkaline), with elevated heavy rare earth element concentrations and anonymously negative Eu values. Pervasive spongy groundmass and recrystallization textures are consistent with the elevated and remobilized Zr, Th, and Y + HREE (heavy rare earth element) concentrations and a high field strength element (HFSE) soluble, sub-alkalic, F-rich, magmatic system. REE-bearing minerals are present as late-magmatic, interstitial phases and attributed with closed-system, post-magmatic, hydrothermal alteration. Petrogenetic modeling provides scenarios that explain the geochemical evolution and REE complexing behavior in evolved rhyolite magmas, and determines possible source compositions and evolution. Trace element models suggest a system typical of having extensive magmatic differentiation. The resulting rhyolite magma is indicative of a silica-rich magmatic system enriched in H_2O, Li, and/or F that could be considered transitional between pure silicate melt and hydrothermal fluid, where fluorine-ligand complexing was prevalent through late magmatic cooling and crystallization processes. Thorough differentiation and high fluorine activity contributed to the late stage crystallization of REE-bearing minerals in the Round Top rhyolite.

Keywords: petrology; geochemistry; rhyolite; rare earth elements; petrogenesis

1. Introduction

The Trans-Pecos region of Texas hosts more than 100 Paleocene to Miocene age intrusive igneous and extrusive bodies related to subduction and later rifting along the southwest margin of North America. Many of the localities, including Round Top and the other laccoliths of the Sierra Blanca Complex (SBC) are hypabyssal, sub-volcanic, and rhyolitic in composition. Despite the numerous magmatic rocks in the Trans-Pecos area and contiguous regions, only a few have been analyzed for rare earth element (REE) geochemistry and recognized to have REE mineral occurrences.

The Round Top rhyolite is enriched in Be, F, Li, Nb, Rb, Sn, Th, U, Y, Zr, and REEs [1–4]. REE-bearing minerals are mainly ubiquitous nano-scale accessory phases throughout the groundmass, including Y- and Ce-rich fluorite, columbite-(Fe), synchysite-group minerals, xenotime-(Y), and zircon. The rhyolite is composed of 45–50% K-feldspar, 25–30% quartz, 10–15% albite plagioclase, 3–7% biotite, and 1–3% opaque oxides (by volume). The rhyolite is slightly peraluminous, silica-rich, sub-alkalic, with elevated HREE concentrations and a negative Eu-anomaly. The rhyolite has elevated concentrations of Zr, with zircon visible in thin section and SEM (scanning electron microscope) images as primary magmatic and secondary Th-rich metamict vapor/hydrothermal phases. This is

consistent with a HFSE soluble, sub-alkalic and fluorine-rich, magmatic system. REEs are incorporated throughout interstitial groundmass and attributed with late-magmatic mineralization and transitional post-magmatic hydrothermal/vapor phase alteration.

A comprehensive petrogenetic model provides possible scenarios for the geochemical evolution and REE complexing behavior in evolved rhyolitic rocks, and determines whether magmatic crystal fractionation or precipitation from hydrothermal fluids was the main mechanism for HREE-enrichment and mineralization. Round Top is one of the few well studied Tertiary igneous bodies in west Texas. Geochemical modeling of laccoliths in the SBC shows the potential source and evolution of similar igneous laccoliths across west Texas, and illustrates the REE resource potential of differentiated rhyolite magmas in the Trans-Pecos Igneous Province.

2. Geologic Setting

The Sierra Blanca Complex is located in west Texas, in the Trans-Pecos Magmatic Province (TPMP; Figure 1). The rhyolites were emplaced along limestone and shale bedding planes of the Buda limestone and Del Rio Clay of the Washita Group strata. The crystalline limestone and marly clay country rocks are poorly exposed and typically covered by Quaternary arroyos and alluvial fan sediments. Magmatism within the region is bimodal, ranging from basaltic and gabbroic mafic compositions to highly evolved silicic rhyolite [3,5–7]. Igneous bodies in the TPMP range from extensive caldera-sourced pyroclastic deposits to sills, dikes, and shallow laccoliths [3,8,9]. The TPMP igneous compositions can be separated into two geochemical districts—predominantly alkali-calcic toward the west, and alkalic compositions to the east [8,10,11].

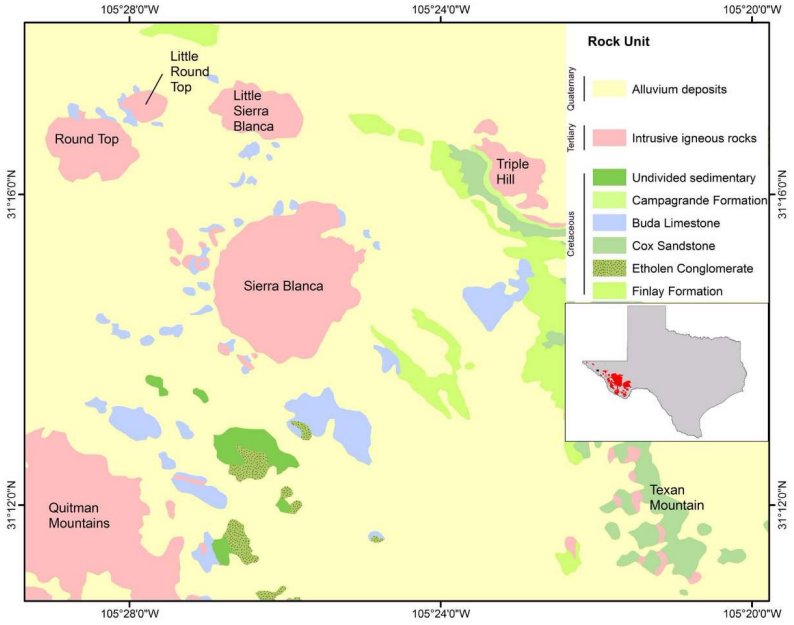

Figure 1. Generalized geologic map of the Sierra Blanca Complex and surrounding rhyolite laccoliths, including the Round Top rhyolite (adapted from [16]). Inset map of Texas shows the location of the SBC (black square) and the extent of the Trans-Pecos Magmatic Province (red shapes; adapted from [16]) in west Texas.

Magmatism in the region occurred between 100 and 40 Ma ago, related with the subduction of the Farallon plate under the North American continent. Bimodal volcanism extended east from the west coast subduction zone [3,12]. Trans-Pecos magmatism occurred 48–17 Ma and is separated into early and later phases [3,6,7,13]. The early phase (48–38 Ma) is characterized by voluminous silicic to mafic igneous intrusions, lava flows, and caldera eruptions [3,6]. The late phase (38–32 Ma) was compositionally variable, ranging from alkali–calcic to alkalic, and represents the most active

magmatism in the region [3,5,6,10]. The Sierra Blanca laccolith, adjacent to and associated with Round Top, was emplaced during the main phase of bimodal TPMP activity at 36.2 ± 0.6 Ma (K/Ar in biotite; [4]). Volcanism during this period is characterized by silicic to mafic intrusions, and large-volume caldera eruptions associated with voluminous ash-flow tuffs [3,6,8]. Basin and Range extension was initiated by a change in the region's stress around 31 Ma, and extensive normal faulting initiated around 24 Ma [3]. Mafic volcanism in the early stages of rifting has been dated at 17 Ma [3].

Sierra Blanca Complex

The Sierra Blanca Complex comprises five separate rhyolite and rhyolite porphyry laccoliths. SBC laccoliths are aphanitic to slightly porphyritic, and are located in a 90 km^2 area about 18 km southeast of the Finley Mountains (47 Ma) and 5 km north of the Quitman Mountains (35 Ma; [6]). The largest laccolith, Sierra Blanca, was emplaced 36.2 ± 0.6 Ma [6]. Emplacement ages of the other SBC laccoliths have not been measured, but a relative emplacement sequence can be interpreted through major- and trace-element differentiation. The increasing enrichment of REEs, especially the increasing ratio of HREEs to LREEs (light rare earth elements) between laccoliths, suggests that Triple Hill was emplaced first, followed by Sierra Blanca, Round Top, Little Sierra Blanca, and Little Round Top [3,14–16]. The slight differences in compositions and rapid cooling textures suggest the timing between emplacement and duration of emplacement was relatively short.

Sierra Blanca is the largest of the SBC laccoliths. The laccolith is pink to gray in color, chemically and texturally homogenous and composed of quartz rhyolite porphyry. Alteration of the rhyolite is not pervasive compared to Round Top, but hematitic and manganese oxide staining is evident throughout jointed and faulted portions of the laccolith. Round Top is the most westerly of the SBC (Figure 1) and comprise four variations of rhyolite that differ slightly by color, mineralogy, and texture. The rhyolite is fragmented, heavily jointed, blocky, and locally cemented by multiple generations of fluorite, calcite, and quartz.

Several sills and dikes outcrop around and within the SBC laccoliths. These intrusions precede the main laccolith magmatism and are composed of hypabyssal hornblende andesite porphyry, porphyritic diorite, and latite porphyry dikes [17–20]. Diorite to andesitic dikes and sills from around Sierra Blanca and Round Top were dated at 40.6 ± 0.1 Ma (K/Ar age; [19]). A sill outcropping along the northern margin of Round Top is hornblende diorite porphyry and sits unconformably beneath the laccolith. Parts of the sill and surrounding limestone are partially brecciated and fluoritized. Whether the dikes and sills have any relationship to the Round Top mineralization is unclear, but it is probable that the same magmatic conduits that emplaced the sills were used during emplacement of SBC laccoliths.

3. Materials and Methods

More than 350 samples were collected from Round Top, Little Round Top, and Sierra Blanca. Samples were collected from outcrops, road cuts and drill cuttings obtained during exploratory drilling by Texas Mineral Resources Corporation. Petrographic work on more than 40 thin sections was conducted using petrographic microscopes. Thin sections were made to the standard thickness of 30-microns. Microbeam analyses were conducted in the University of Austin at Texas, Department of Geological Sciences (Austin, TX, USA), Electron Microbeam Laboratories on a JEOL JXA-8200 Electron Microprobe.

Samples from Round Top were analyzed at a commercial facility (ACMELABS, Vancouver, BC, Canada; see Appendix B for blind duplicate analyses). Samples of ~10 kg from each locality were broken into smaller unweathered pieces and combined into a single sample of ~5 kg. Each sample was jaw-crushed, and splits pulverized in a carbon-steel ball-mill. Major elements were prepared with $LiBO_2$ fusion and analyzed by X-ray fluorescence (XRF). Detection limits for major elements were 0.01 wt %, and 0.1% loss on ignition (LOI). For trace and rare earth elements, a multi-acid digestion was

conducted where 0.25 g was heated in HNO_3–$HClO_4$–HF and dried. The residue was dissolved in HCl and analyzed by inductively couple plasma mass spectroscopy (ICP-MS). Detection limits for SiO_2, Al_2O_3, MgO, CaO, Na_2O, K_2O, TiO_2, P_2O_5, Li, FeO and MnO were 0.01 wt %; Fe_2O_3 was 0.04 wt %; Cr_2O_3 was 0.02 wt %. Detection limits for Sc, Ba, Be, Sn, and Zn were 1 ppm; Co and Th were 0.2 ppm; Cs, Hf, Nb, Rb, Ta, U, Zr, Y, La, Ce, Mo, Cu, Pb, Ni, Cd, Sb, Bi, Ag and Tl were 0.1 ppm; Ga, Sr, W, As, Au and Se were 0.5 ppm; V was 8 ppm; Pr, Eu and Ho were 0.02 ppm; Nd was 0.3 ppm; Sm, Gd, Dy and Yb were 0.05 ppm; Tb, Tm, Lu and Hg were 0.01 ppm; Er was 0.03 ppm. F was analyzed separately by specific ion electrode, with a detection limit of 0.01 vol %.

4. Results

4.1. Mineralogy

Phenocryst and groundmass typically comprise equal proportions of the rhyolite (50% phenocrysts, 50% groundmass; Figure 2). Plagioclase feldspar comprises less than 15% of the rhyolite as subhedral to euhedral, rectangular (smaller than 0.5 × 1.2 cm), albite lathes, commonly with K-feldspar overgrowths. These lathes occur in clusters, as penetrating twins, or as individual phenocrysts, and occasionally K-feldspar mantles have their own albite overgrowths. The albite before the potassium feldspar overgrowth is typically equant without reaction textures, indicating a lack of dissolution before the formation of the K-feldspar. Potassium feldspar constitutes about 45–55% of the rhyolite and is found as 0.75–2 cm phenocrysts with hourglass sector zonation, or as mantles around early formed sodic plagioclase (Figure 3). Quartz comprises about 25–35% of the rhyolite, occurring as zoned, anhedral to subhedral 0.2–1.5 cm phenocrysts. The core is typically equant, euhedral to subhedral, early beta quartz, pseudomorphed to trigonal, low temperature, alpha quartz. Quartz typically exhibits pseudo-concentric rings (snowball texture), where repeated corrosion and crystallization of later quartz overgrowths occurred. Biotite is annitic and comprises less than 5% of the rhyolite. The annite occurs as interstitial subhedral to anhedral phenocrysts less than 1 mm in size, displaying moderate pleochroism, alternating from a greenish-yellow to dark brown-green, where the edges of are commonly irregular, ragged, and undulatory, filling the space between earlier phenocrysts.

Minor phases comprise less than 10% of the rhyolite, including magnetite, hematite, and zircon. Magnetite and hematite comprise 2–3% of the rhyolite, where hematite is directly related to oxidation. Magnetite occur as euhedral to subhedral 0.1–1.5 cm phenocrysts, and as micro-crysts in the groundmass. Magnetite is typically found as anhedral inclusions in other phenocrysts, ranging from 1–5 mm in size, in close association with other accessary phases, including cassiterite, changbaiite ($PbNb_2O_6$), columbite-(Fe) group minerals, zircon and Y ± REE fluorides. Hematite occurs as replacement around the edges of magnetite phenocrysts, and less than 1–2 μm inclusions within the K-feldspar groundmass.

Trace minerals include zircon, Y-REE-fluorides, cassiterite, cerianite-(Ce), changbaiite, columbite-(Fe), cryolite and thorite. Zircon is the most common trace mineral, approximately 0.5–1% of the rhyolite at Round Top. Two populations of zircon are distinguished: one has abundant thorite inclusions and in the other these inclusions are rare. Most grains are 0.1–0.4 mm anhedral to subhedral, occasionally euhedral, phenocrysts. Rubin et al. [21] hypothesized the two zircon populations represent an early magmatic (thorite inclusion-rich), and a later population introduced by migrating hydrothermal fluids (thorite inclusion-poor). Ref. [21] noted the ubiquitous presence of late-stage hydrothermal zircons within fluorite replacement in surrounding limestone, but not within Round Top rhyolite. Both zircon populations (thorite inclusion-rich and inclusion-poor) were observed in Round Top rhyolite, commonly in close proximity to each other.

Yttrofluorite ((Ca, Y, HREE)F_2), yttrocerite ((Ca, Y, Ce, LREE, HREE)F_2) and variations that include La, Th, Nd, Dy, Yb, Lu, and Tm are the main REE-fluorides identified within Round Top rhyolite (Figure 4). Additional REE-bearing minerals have been observed and detailed in other

papers [3,16,22], including aeschynite-(Ce), synchysite-group minerals, Nb-REE and Ca–Th-REE fluorides. The REE-fluorides and other trace minerals are typically nanoscale, anhedral, interstitial, and late crystallizing.

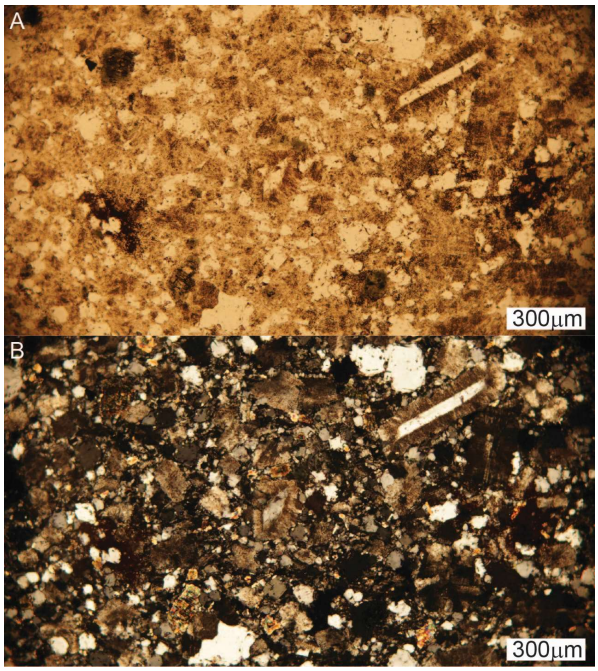

Figure 2. Plane-polarized (**A**) and cross polarized (**B**) transmitted light photomicrographs of Round Top rhyolite (adapted from [23]).

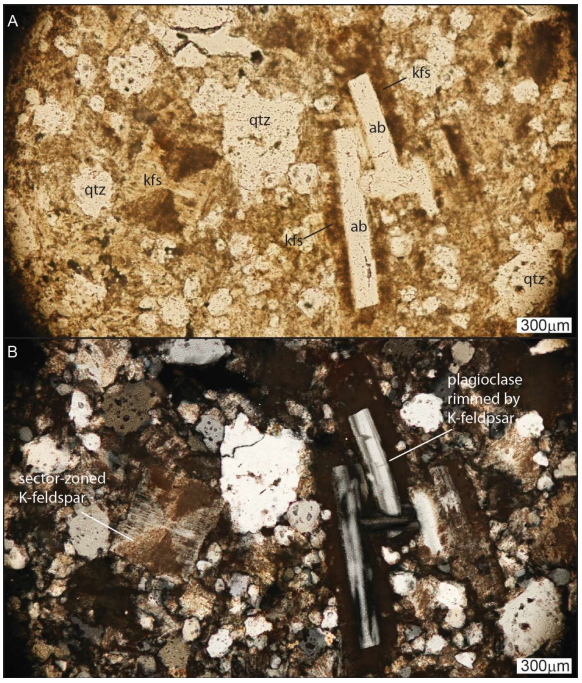

Figure 3. Plane-polarized (**A**) and cross polarized (**B**) transmitted light photomicrographs showing albite (ab), K-feldspar (kfs), quartz (qtz) and groundmass mineral textures in the Round Top rhyolite (adapted from [23]).

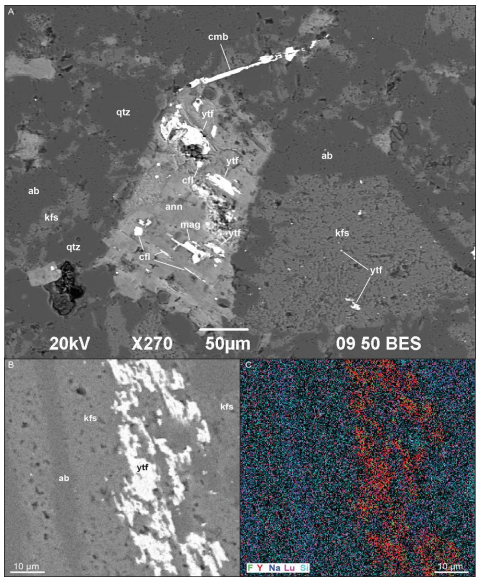

Figure 4. Back-scattered electron images of accessory Y-(ytf; yttrofuorite), Ce-(cfl; cerofluorite), REE-fluoride minerals in the Round top rhyolite, showing the interstitial relationship with annite (ann), columbite (cmb), magnetite (mag), quartz (qtz), albite (ab) and K-feldspar (kfs; (**A**,**B**)) and elemental map distribution by SEM-EDS (**C**) (adapted from [23]).

4.2. Geochemistry

The Round Top laccolith comprises relatively homogenous, high silica, non-topaz bearing rhyolite with low MgO and CaO, high Na_2O and K_2O (Figure 5; Table 1), and relatively high Zr (960–1100 ppm), Rb (1660–1930 ppm), Th (160–190 ppm), and U (28–58 ppm; Table 2). Felsic rocks from the Round Top and Sierra Blanca suite of rocks show predominantly Within Plate (WPG) tectonomagmatic affinity (Figure 6), they are F-rich (up to 2.4 wt %), peraluminous with ASI ratios (Aluminum Saturation Index) around 1.2, but not peralkaline as is typical of many REE enriched systems (Figure 7). Initial Sr^{87}/Sr^{86} ratios for the mafic constituents of the magmatic suite are around 0.702 [19], where values of felsic members are around 0.728 [15]. These contrasting ratios imply a more crustal source for the felsic rocks. The Rb/Sr system appears to be affected by late- to post-magmatic processes increasing Rb relative to Sr (Figure 8). The post magmatic process makes it difficult to rely on Sr in determining crustal contribution to the source of these magmas.

Each of the rhyolite laccoliths of the SBC and other regional magmatic rocks have distinct geochemical characteristics that help to discriminate them from each other [14,15,19]. The Finlay Mountains represent nearby mafic to intermediate compositions (40–65 wt % SiO_2), conforming temporally and compositionally to early gabbro/diorite dikes in the immediate SBC area. The Texan Mountain rhyolite represents the lowest silica content from felsic rocks in the magmatic series (64–70 wt % SiO_2), followed by Triple Hill and Sierra Blanca with Round Top, Little Blanca and Little Round Top representing extremely evolved rhyolitic compositions (70–76 wt % SiO_2). These evolved compositions show an increase in Na_2O relative to K_2O, decreasing Al_2O_3 and very low MgO and P_2O_5 (Figure 5).

Alkalinity Index versus Aluminum Saturation Index show that all of the igneous rocks in the SBC and the Finlay mountains are alkalic, and all but the more primitive Finlay mountains samples are peraluminous. Tectonomagmatic affinity diagrams including Ta vs. Yb suggest a within-plate tectonic setting for the rhyolites from the SBC (see Figure 6), including the samples from Round Top. Rb/Sr ratio versus weight percent oxide of silicon shows a significant enrichment in rubidium for late stage, highly evolved rhyolites in the Sierra Blanca magmatic complex, as Rb fractionates preferentially into residual melts (Figure 8).

Rare earth element plots show LREE enrichment for felsic, intermediate and low SiO_2 rocks in the SBC. Mafic/Intermediate patterns show little to no Eu anomaly, but felsic members are enriched in HREEs and show a moderate to strongly negative Eu anomaly (Round Top, Sierra Blanca, Little Round Top and Little Blanca rhyolites; Figure 9).

Finlay Mountain andesitic basalts, gabbroic/dioritic sills in the SBC area and Texan Mountain have LREE-enriched patterns with negligible Eu anomalies (~0.6) and La/Yb ratios ranging from 18–25, 11 and 10, respectively (Table 3; Figure 9). Triple Hill, Sierra Blanca and Round Top have increasing HREE, and total REE + Y, concentrations and pronounced negative Eu anomalies. Triple Hill samples have total REE + Y concentration of as high as 373 ppm, with average La/Yb ratio of 3 and Eu/Eu* of 0.09 (Eu/Eu* = Eu/[(Sm + Gd)/2]). Sierra Blanca and Round Top have total REE + Y values as high as 356 and 560, with average La/Yb ratios 0.79 and 0.31, and Eu/Eu* 0.19 and 0.14, respectively. Little Round Top and Little Blanca have similarly elevated HREE concentrations, with total REE + Y as high as 558 and 356 ppm, respectively. Average La/Yb ratios for Little Blanca and Little Round Top are 0.44 and 0.31, with average Eu/Eu* ratio of 0.22 (for both laccoliths).

Table 1. Major element compositions (wt %) from the Round Top rhyolite and adjacent rocks.

Sample	**262-01**	**37-01**	**263-02**	**270-03**	**266-01**	**41-01**	**270-02**	**33-02**
Rock Type	**Rhyolite**	**Rhyolite**	**Rhyolite**	**Rhyolite**	**Rhyolite**	**Rhyolite**	**Rhyolite**	**Rhyolite**
SiO_2	74.50	73.17	73.69	73.62	73.52	73.25	73.25	74.31
Al_2O_3	13.31	13.51	13.49	13.50	13.75	13.59	13.33	13.28
Fe_2O_3	1.05	1.05	1.03	1.13	1.02	1.03	1.41	1.29
FeO	0.55	0.59	0.54	0.55	0.51	0.59	0.75	0.50
MgO	0.07	0.27	0.03	0.03	0.11	0.19	0.10	0.03
CaO	0.10	0.25	0.42	0.51	0.14	0.26	0.13	0.12
Na_2O	4.82	4.99	4.69	4.82	4.92	4.93	4.69	4.82
K_2O	4.28	4.16	4.32	4.20	4.40	4.37	4.03	3.95
TiO_2	0.02	0.02	0.02	0.02	0.02	0.02	0.02	0.02
P_2O_5	<0.01	<0.01	<0.01	0.02	<0.01	<0.01	<0.01	0.02
MnO	0.07	0.06	0.06	0.06	0.05	0.07	0.06	0.06
Cr_2O_3	<0.002	<0.002	<0.002	<0.002	<0.002	0.00	<0.002	<0.002
LOI	0.80	1.50	1.30	1.10	1.10	1.20	1.80	1.20
Sum	99.53	99.52	99.56	99.54	99.50	99.49	99.57	99.56
A/CNK *	1.04	1.03	1.03	1.01	1.05	1.02	1.08	1.07
A/NK *	1.06	1.06	1.09	1.08	1.07	1.06	1.10	1.09
Sample	**46-01**	**44-20**	**44-21**	**43-04**	**270-14**	**248-13**		
Rock Type	**Rhyolite**	**Rhyolite**	**Rhyolite**	**Gabbro**	**Fluoritized Limestone**	**Limestone Breccia**		
SiO_2	73.62	73.69	73.78	52.07	4.00	14.50		
Al_2O_3	13.91	13.84	13.98	17.18	0.61	9.94		
Fe_2O_3	1.18	0.39	0.46	4.68	0.20	0.03		
FeO	0.51	0.36	0.44	2.80	0.29	0.30		
MgO	0.10	0.05	0.04	3.70	0.49	0.07		
CaO	0.04	0.41	0.40	6.02	64.97	50.67		
Na_2O	4.83	4.95	4.75	5.16	0.25	0.65		
K_2O	4.20	4.42	4.67	2.81	0.11	0.63		
TiO_2	0.02	0.02	0.02	1.15	0.03	<0.01		
P_2O_5	<0.01	<0.01	<0.01	0.57	<0.01	<0.01		
MnO	0.05	0.03	0.04	0.16	0.04	0.05		
Cr_2O_3	<0.002	<0.002	<0.002	0.00	0.00	<0.002		
LOI	1.10	1.50	1.00	3.20	5.40	12.40		
Sum	99.55	99.62	99.62	99.48	76.43	89.27		
A/CNK *	1.11	1.01	1.03	0.76	0.01	0.11		
A/NK *	1.11	1.07	1.09	1.49	1.15	5.68		

* molecular $Al_2O_3/(CaO + Na_2O + K_2O)$ and molecular $Al_2O_3/(Na_2O + K_2O)$.

Table 2. Trace element compositions (ppm) from the Round Top rhyolite and adjacent rocks; bdl = below detection limit.

Sample	262-01	37-01	263-02	270-03	266-01	41-01	270-02	33-02
Rock Type	**Rhyolite**	**Rhyolite**	**Rhyolite**	**Rhyolite**	**Rhyolite**	**Rhyolite**	**Rhyolite**	**Rhyolite**
Li	500	400	300	500	600	400	500	500
F	2200	900	400	4800	3100	5500	2400	2300
Sc	1	bdl	bdl	1	bdl	bdl	bdl	bdl
Ba	11	13	19	119	221	58	7	57
Be	47	42	35	39	26	55	10	12
Co	0	0	0	0	1	0	1	1
Cs	62	56	60	61	39	51	40	47
Ga	71	71	68	70	71	70	72	68
Hf	81	81	77	81	80	78	73	84
Nb	363	350	348	352	359	363	369	342
Rb	1896	1843	1928	1907	1882	1916	1757	1663
Sn	151	142	138	139	141	135	140	140
Sr	13	152	31	38	62	167	114	26
Ta	59	58	57	58	57	60	57	59
Th	168	176	168	169	173	181	172	167
U	33	30	36	28	32	34	40	31
V	13	bdl	bdl	bdl	12	10	12	bdl
W	4	3	3	3	4	5	4	4
Zr	1046	1060	1003	1041	1050	1084	969	1083
Y	105	188	106	147	175	223	160	137
Mo	1	1	1	0	1	1	1	0
Cu	1	1	1	2	1	1	1	1
Pb	67	78	83	48	221	182	58	83
Zn	624	516	604	581	546	553	501	520
Ni	1	1	1	2	2	1	1	1
As	12	7	9	9	8	5	2	4
Sb	2	1	1	2	2	1	2	1
Bi	2	2	2	3	3	3	3	2
Tl	1	2	1	1	1	2	2	1

Sample	46-01	44-20	44-21	43-04	270-14	248-13
Rock Type	**Rhyolite**	**Rhyolite**	**Rhyolite**	**Gabbro**	**Fluoritized Limestone**	**Limestone Breccia**
Li	500	400	500	bdl	bdl	bdl
F	2400	2900	3900	1100	342700	193300
Sc	bdl	1	1	13	bdl	8
Ba	21	9	7	2294	54	160
Be	17	19	6	13	3898	205
Co	0	0	1	19	2	2
Cs	50	43	44	84	9	8
Ga	71	67	66	19	2	15
Hf	79	77	80	5	0	12
Nb	362	368	378	10	1	59
Rb	1857	1801	1902	130	31	265
Sn	143	144	153	bdl	1	23
Sr	21	41	34	1063	1771	784
Ta	59	61	62	1	0	9
Th	165	161	162	8	1	35
U	47	58	53	2	124	365
V	10	bdl	bdl	180	25	23
W	5	3	4	1	6	1
Zr	1052	999	1038	172	10	166
Y	203	101	106	21	25	189
Mo	0	0	0	0	1	1
Cu	1	1	0	24	1	1
Pb	148	126	135	7	389	353
Zn	487	136	159	43	158	152
Ni	1	0	1	6	bdl	bdl
As	7	2	2	1	33	51
Sb	2	1	1	bdl	1	0
Bi	1	1	0	bdl	0	1
Tl	2	2	2	bdl	0	1

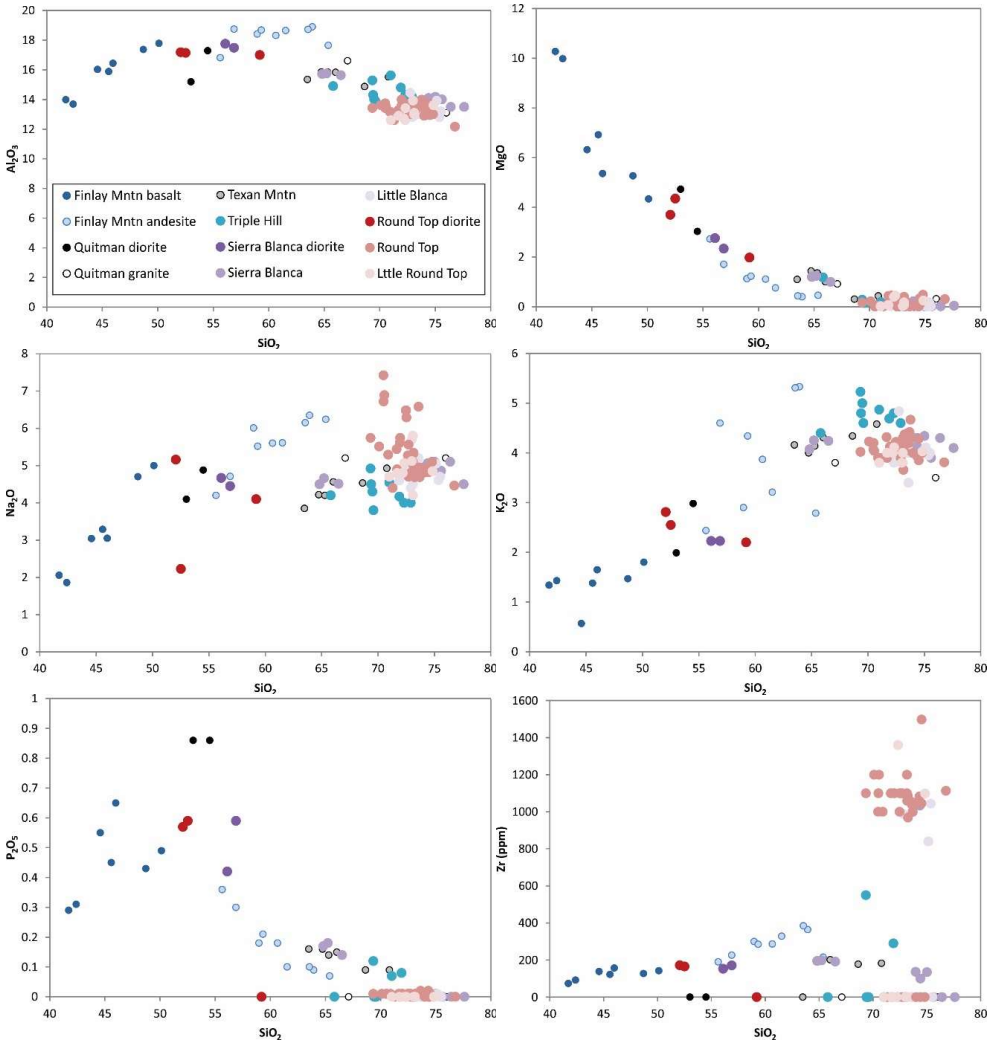

Figure 5. Major element (wt %) and trace element (ppm) vs. SiO_2 (wt %) concentrations in rhyolite from Round Top and other laccoliths in the Sierra Blanca Complex, compared with other regional igneous rocks from the Quitman mountains and Finlay mountains [14,15,19].

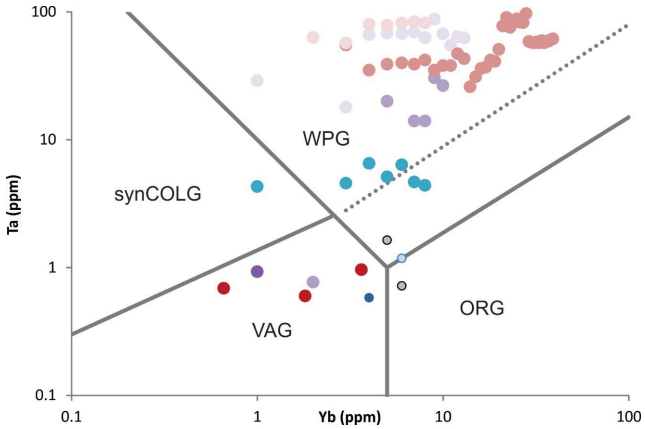

Figure 6. Tectonomagmatic affinity plot [26] of Ta vs. Yb, showing the within-plate affinity of the Round Top rhyolite compared to other igneous rocks of the Sierra Blanca Complex, the Quitman mountains and Finlay mountains [14,15,19]. Symbology is the same as Figure 5.

Table 3. Rare earth element compositions (ppm) from the Round Top rhyolite and adjacent rocks.

Sample	262-01	37-01	263-02	270-03	266-01	41-01	270-02	33-02
Rock Type	Rhyolite	Rhyolite	Rhyolite	Rhyolite	Rhyolite	Rhyolite	Rhyolite	Rhyolite
La	19.00	20.80	16.80	16.80	19.50	20.10	22.70	20.50
Ce	85.30	73.00	66.10	70.50	59.90	70.00	72.00	58.60
Pr	8.42	9.81	8.04	8.04	9.27	10.31	10.85	9.87
Nd	24.50	24.10	23.70	24.40	26.70	24.60	28.00	26.50
Sm	6.31	7.82	6.78	7.37	8.52	9.92	8.34	8.04
Eu	0.09	0.09	0.05	0.11	0.13	0.10	0.10	0.10
Gd	5.38	7.90	6.38	7.27	8.59	9.95	7.25	6.56
Tb	1.74	2.82	2.03	2.49	2.76	3.65	2.30	2.16
Dy	16.94	24.21	17.33	22.38	24.82	31.71	22.10	19.00
Ho	4.15	6.83	4.22	5.36	6.47	8.04	5.62	4.83
Er	18.57	28.82	18.37	22.73	27.39	33.12	25.01	21.06
Tm	4.37	6.51	4.35	4.80	6.05	6.91	5.88	5.08
Yb	39.13	52.56	35.22	41.26	50.09	58.01	48.95	45.19
Lu	6.31	8.26	5.89	6.17	7.69	8.67	7.76	7.06
Sample	**46-01**	**44-20**	**44-21**	**43-04**	**270-14**	**248-13**		
Rock Type	**Rhyolite**	**Rhyolite**	**Rhyolite**	**Gabbro**	**Fluoritized Limestone**	**Limestone Breccia**		
La	7.40	6.20	2.20	32.60	2.80	5.80		
Ce	29.00	25.90	15.60	61.90	3.90	15.10		
Pr	3.97	2.96	1.56	7.56	0.52	2.84		
Nd	10.90	9.90	6.30	30.30	1.00	8.50		
Sm	5.24	3.81	2.86	6.19	0.60	4.39		
Eu	0.07	<0.02	0.05	1.96	0.14	0.13		
Gd	7.55	4.00	4.18	5.47	0.82	7.77		
Tb	3.03	1.89	1.81	0.73	0.29	3.13		
Dy	28.38	20.27	17.67	4.64	2.97	28.01		
Ho	7.44	5.17	5.03	0.81	0.77	6.63		
Er	30.99	22.45	24.19	2.18	3.42	25.45		
Tm	6.64	5.33	5.49	0.30	0.58	4.78		
Yb	54.16	46.15	48.38	1.81	3.70	31.56		
Lu	8.09	7.04	7.58	0.29	0.52	4.36		

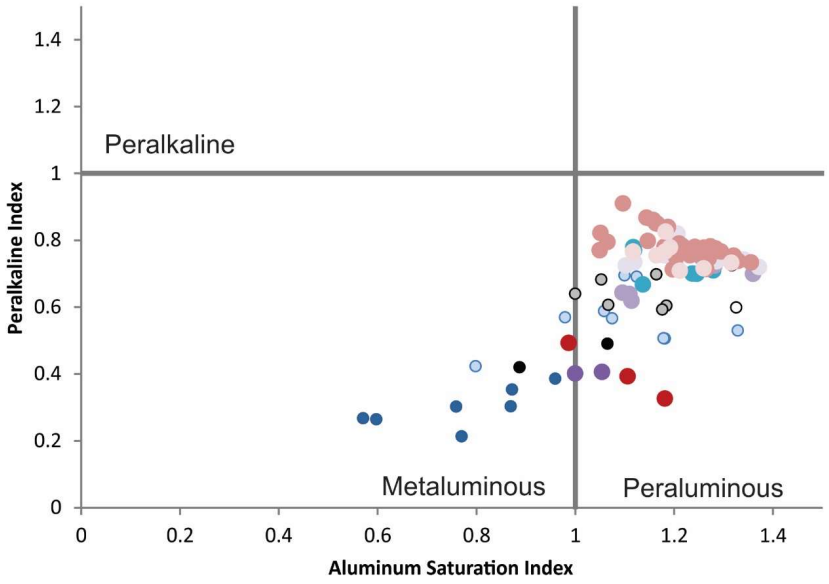

Figure 7. Aluminum Saturation Index (molar ratio $Al_2O_3/CaO + Na_2O + K_2O$) vs. Alkalinity Index (molar ratio $Al_2O_3/Na_2O + K_2O$) of Round Top rhyolite compared to other laccoliths of the Sierra Blanca Complex, the Quitman Mountains and Finlay Mountains. Symbology is the same as Figure 5.

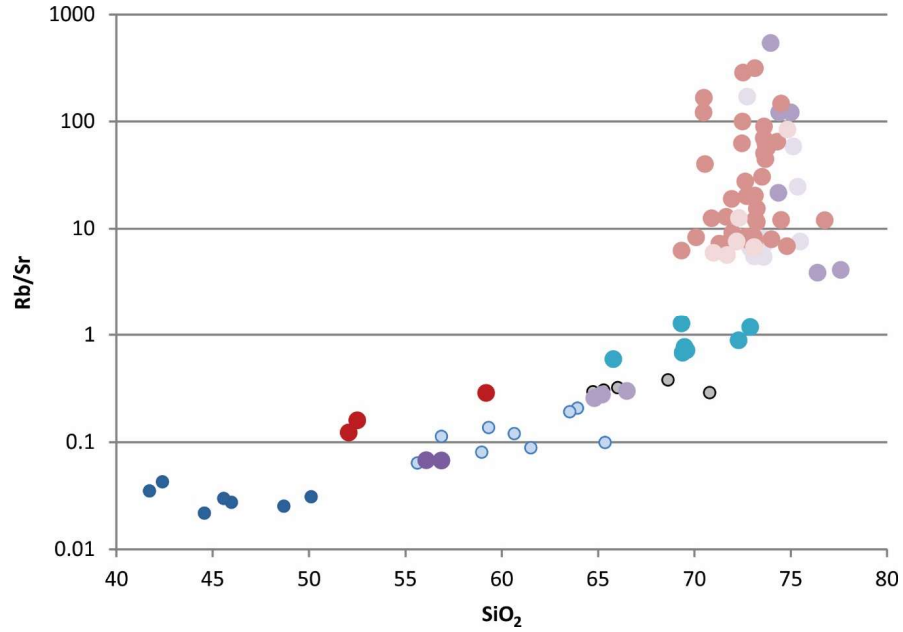

Figure 8. Rb/Sr vs SiO_2 (wt %) of the Round Top rhyolite compared to other igneous rocks of the Sierra Blanca Complex, the Quitman mountains and Finlay mountains [14,15,19]. The Round Top rhyolite shows extreme differentiation with very high Rb/Sr ratios, over a couple of orders of magnitude compared to most the other igneous rocks. Symbology the same as Figure 5.

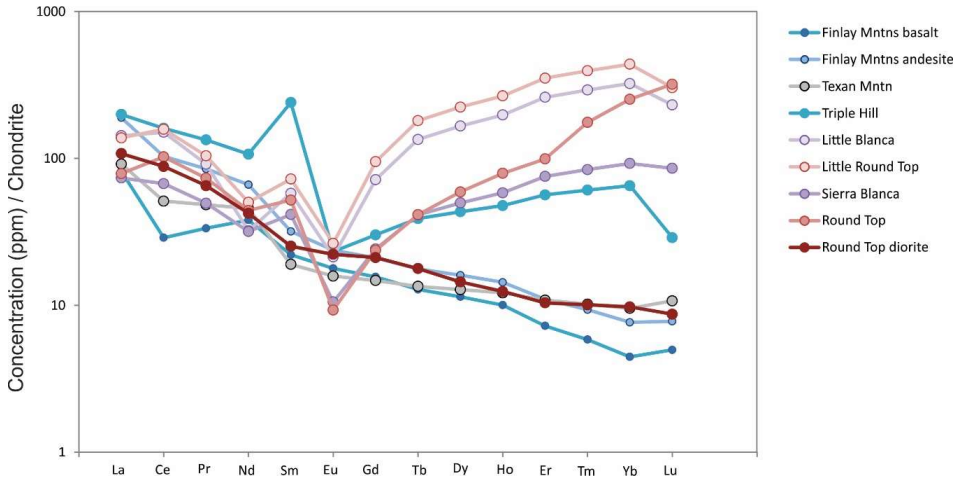

Figure 9. Average chondrite normalized [27] rare earth element plots of separate rhyolite laccoliths and diorite dikes in the Sierra Blanca Complex along with the andesitic basalt and basaltic andesite from the Finlay Mountains [14,15,19].

4.3. Geochemical Modeling

The rhyolite of the Round Top laccolith does not have any direct source material indicators (autoliths, xenoliths, etc.) and identification of protolith compositions is determined from indirect geochemical and isotopic constraints, and petrogenetic modeling of probable regional source rocks. The Finlay Mountain andesitic to basaltic compositions represent earlier more primitive magmas that could be differentiated to form rhyolite similar to Round Top. The variation in Sr isotope ratios between mafic sills in the SBC (Sr^{87}/Sr^{86} = 0.702) [19] and Round Top (Sr^{87}/Sr^{86} = 0.728) [15], may be the result of late- to post-magmatic and hydrothermal processes that effected the Rb/Sr system. It is possible that crustal melts contributed, at least partially, to the initial melts that produced the Round Top rhyolite. Granulitic crustal rocks in the Trans-Pecos region provide possible source material at

depth. Mafic, intermediate, and felsic xenolith compositions have been identified in the Trans-Pecos region and represent crustal lithologies [24].

The petrogenetic model evaluates starting melts of a composition similar to the andesitic basalts of the Finlay Mountains, differentiated by closed-system Rayleigh fractional crystallization (FC) to produce early Sierra Blanca Complex melts—compositions similar to Texan Mountain and Triple Hill, and crustal melts represented by xenoliths from the Trans-Pecos region (Figure 10a). Solid lines represent the differentiation sequence of a range of regional basaltic compositions, dotted line represents batch melting (BM) of a range of regional crustal xenolith sources. Both products of regional melted crust and differentiated mafic magma compositions can produce appropriate melts similar to the mafic diorite sills that precede the Round Top rhyolite in the Sierra Blanca Complex, though major element least sum-residual-squared regression [25] of Tran-Pecos crustal xenolith (Σrisidual^2 = 1.003 at 33.70% melt) and Finlay Mountain andesitic-basalt (Σr^2 = 10.265 at 28.12% fractionation) mineralogies suggests a crustal melt is more appropriate for the rhyolite source.

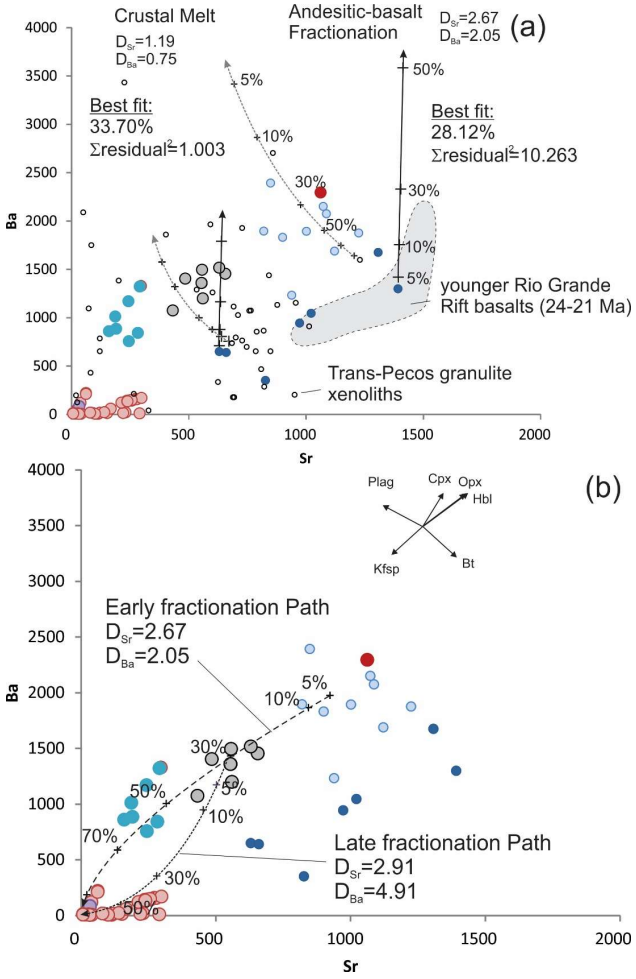

Figure 10. (**a**) Petrogenetic model showing the change in Ba vs. Sr composition for a range of Finlay Mountain basalt compositions (blue circles). Solid lines represent the differentiation sequence of a range of Finlay Mountain basaltic compositions, dotted line represents batch melting (BM) of a range of Trans-Pecos granulite xenolith sources [24] (small open circles) melted at incremental percentages. Round Top mafic dike/sill compositions (red circle) represent the most primitive of SBC compositions. (**b**) The fractionation of the early phenocryst assemblage producing Sr and Ba melt compositions similar to Texan Mountain at 30% (grey circles), Triple Hill at about 50% and late fractionating phenocryst assemblage producing compositions similar to Round Top at 50–90% fractionation of a Texan Mountain or Triple Hill intermediate to felsic compositions (modeling parameters described in Appendix).

The sum residual squared from differentiated andesitic basalt, or melted crust, shows good correlation when compared with rare earth patterns for Round Top diorite compositions (i.e., The diorite compositions correlate well with melted xenolith (r^2 = 0.9551) and fractionated basalt compositions (r^2 = 0.9753); Figure 11). The FC of the observed early phenocryst assemblage from melt products in the melting model produce compositions similar to Texan Mountain and Triple Hill at 60% FC (Figures 10b and 12). Melt compositions similar to Texan Mountain fractionating observed mineral phases become the highly evolved compositions of Round Top, Sierra Blanca, Little Round Top and Little Blanca between 50% and 90% FC (Figures 10b and 13). The REE model correlates well with early FC modeling, but HREE enrichment starts to effect correlation (r^2 = 0.9353) when modeling compositions from Triple Hill through the most evolved compositions, even though LREEs fit very well.

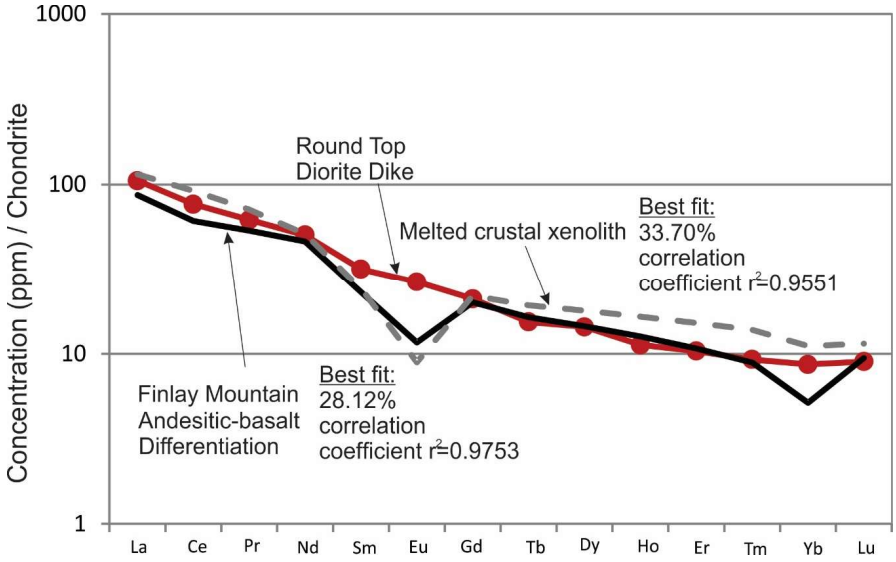

Figure 11. Chondrite normalized [27] rare earth element plots of diorite dikes in the Sierra Blanca Complex compared to the best possible melt compositions of modeled crustal xenolith source rocks (dashed grey line) and differentiation by closed system fractional crystallization of andesitic-basalt compositions (solid black line). Modeling parameters are described in Appendix A.

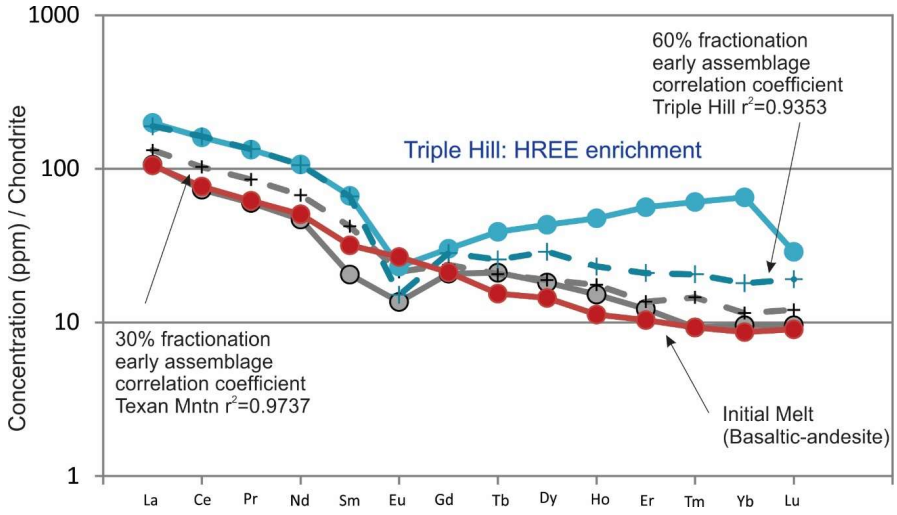

Figure 12. Chondrite normalized [27] rare earth element plots of modeled andesitic basalt dike/sill compositions from the Sierra Blanca Complex (Red circles), Texan Mountain (grey circles) and Triple Hill laccolith (light blue circles) compared to modeled 30% (dashed grey line) and 60% (dashed light blue line) FC of mineral phases from early melt (modeling parameters are described in Appendix A).

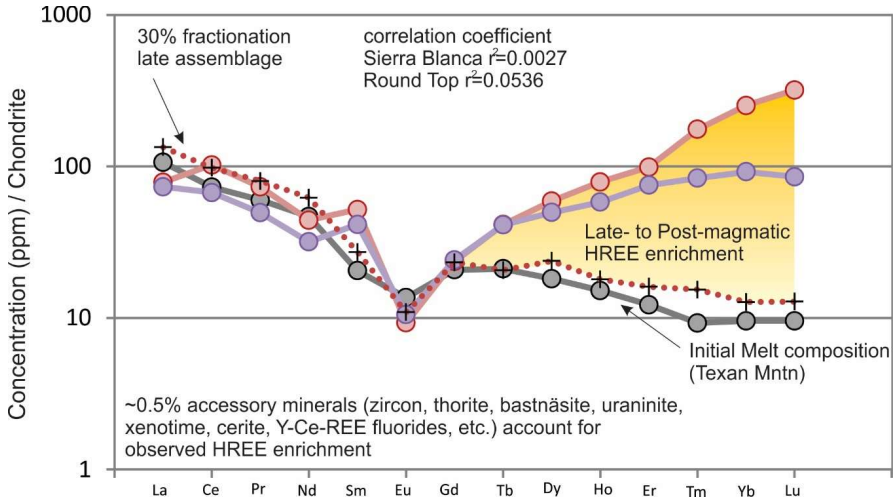

Figure 13. Chondrite normalized [27] rare earth element plots of Texan Mountain rhyolite composition (grey circles) and Sierra Blanca (purple circles) and Round Top (pink circles) compositions compared with 30% late fractionating mineral phases (at 30%; red dotted line). Modeled LREEs correlate well, but HREEs are grossly underestimated (modeling parameters are described in Appendix A).

The significant HREE enrichment in Round Top and Sierra Blanca are difficult to account for with the observed late stage crystallizing phases. A model that incorporates just 0.5% of REE bearing accessory minerals known to be present, but in the matrix as pervasive micro to nano-crystalline crystals, accounts for the observed enrichment. The HREE enrichment is occurring at the transition between late stage magmatic crystallization (with an exsolving vapor phase) and alteration/precipitation related to high-temperature hydrothermal fluids, but with high enough fluorine to retain a large amount of silicate melt component in the fluid. The Round Top rare earth geochemistry is modeled and compared to similar highly evolved systems (Kymi complex in southern Finland [28], Erzgebirge and adjacent Fichtelgebirge and Oberpfalz rocks in Germany [29,30]) to understand the timing and processes that form economically viable rare earth element deposits in highly evolved magmatic rocks (Figures 14–16).

Irber [30] discusses quantification of the tetrad effect and ligand dependent differences in the ionic radii of REEs [32]. The variation in ionic radii are based on variable expansion of the electron cloud (nephelauxetic- or tetrad-effect), type of complexing and internal atomic structure. The inference is that the tetrad effect can be generated during REE partitioning at the transition between silicate melt and high-temperature hydrothermal systems, or between coexisting melt, aqueous high-temperature late stage fluid and crystallizing minerals, in both cases with strong complexing of fluorine and REE.

The tetrad-effect integrates a quantitative measurement of the observed variation in La–Nd, Sm–Gd, Gd–Ho, and Er–Lu trends. The tetrad effects $TE_{1,3}$ are quantified using chondrite normalized values in Irbers equation [30], $TE_{1,3} = (t1 \times t3)^{1/2}$, where $t1 = (Ce/Ce^t \times Pr/Pr^t)^{1/2}$ and $t3 = (Tb/Tb^t \times Dy/Dy^t)^{1/2}$; $Ce/Ce^t = Ce_{CN}/(La_{CN}{}^{2/3} \times Nd_{CN}{}^{1/3})$, $Pr/Pr^t = Pr_{CN}/La_{CN}{}^{1/3} \times Nd_{CN}{}^{2/3})$, $Tb/Tb^t = Tb_{CN}/(Gd_{CN}{}^{2/3} \times Ho_{CN}{}^{1/3})$ and $Dy/Dy^t = Dy_{CN}/(Gd_{CN}{}^{1/3} \times Ho_{CN}{}^{2/3})$. Trace element ratios and tetrad calculations help to determine if the system mineralization was largely charge and radius controlled (CHARAC), derived from magmatic hydrothermal fluids, or transitional non-charge and radius-controlled ligand complexing processes (Non-CHARAC) [30,31,33]. Rb preferentially fractionates into residual melt, and extremely low K/Rb ratios (<50) commonly indicate interaction with an aqueous fluid phase (Figure 14a). Eu and Sr should have similar behavior in granitic systems. The observed decoupled behavior, where Sr is elevated relative to Eu, is a result of strong Eu depletion with early feldspar crystallization (Figure 14b). Zr/Hf ratios shift toward lower ratios with more evolved compositions of silicate melts. Round Top ratios represent increased Hf in late stage zircons transitioning to very low Zr/Hf ratios of pegmatitic systems (e.g., [34]). Y/Ho ratios have near chondritic values, but only coincidently due to an original path of differentiation and non-CHARAC

behavior followed by fluorine ligand complexing in late silicate melt before aqueous fluid transition. Y/Ho ratios combined with Zr/Hf ratios show that the Round Top samples do not have the elevated Y and Hf relative to Ho and Zr, respectively, that would be typical of hydrothermal alteration processes in these types of rocks (cf. [35]; Figures 15 and 16). Y and HREEs were retained in the melt due to the F-rich nature of the magmas (cf. [36–38]).

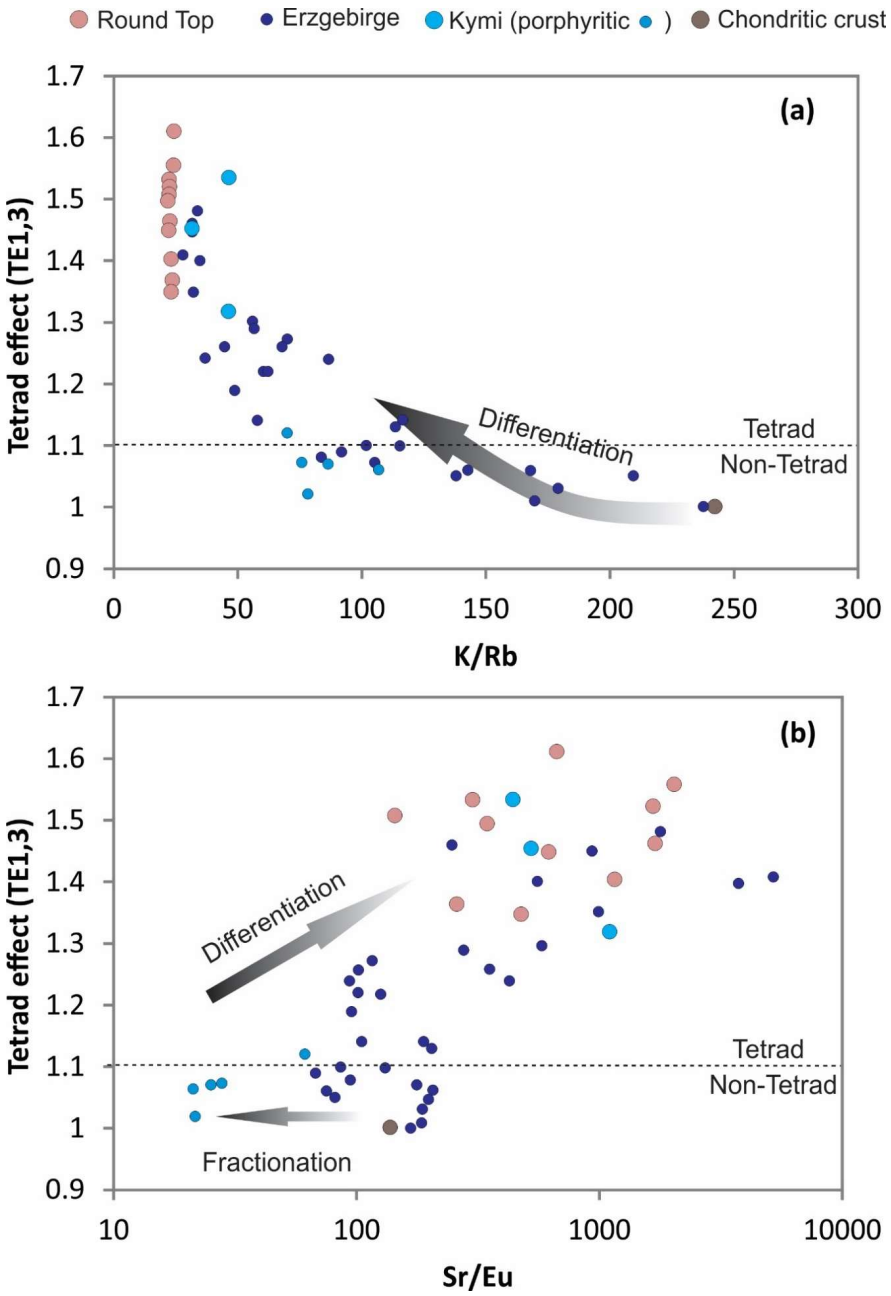

Figure 14. Tetrad-effect vs. (**a**) K/Rb and (**b**) Sr/Eu ratios showing modeled fractionation and differentiation trends (after [30]) and Round Top rhyolite compared with samples from Erzgebirge [29, 30], Kymi [28] and chondritic crust. The tetrad effect shows irregularity from expected REE behavior by comparing the sum of Ce + Pr to La and Nd, and Tb + Dy to Gd and Ho [30].

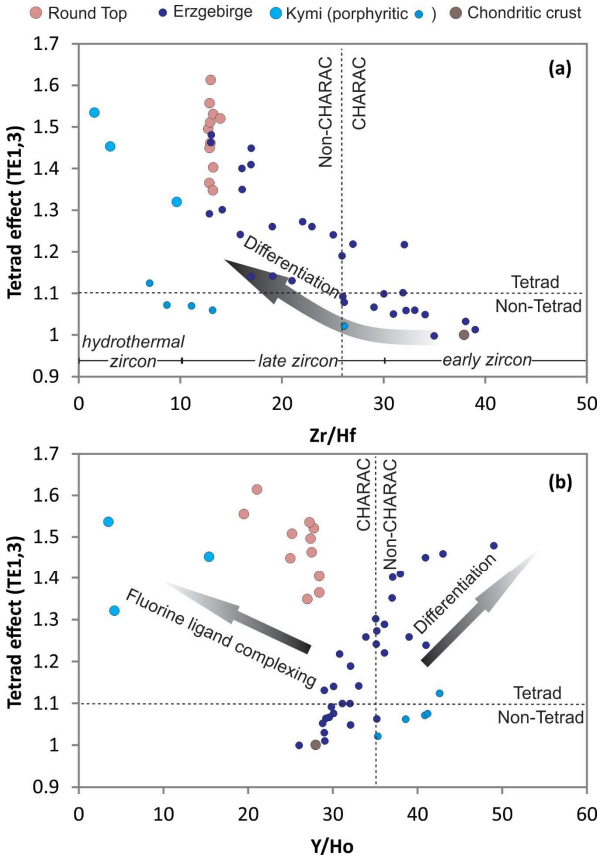

Figure 15. Tetrad-effect vs. (**a**) Zr/Hf and (**b**) Y/Ho ratios showing modeled differentiation and fluorine ligand complexing trends, tetrad vs non-tetrad, CHARAC vs. Non-CHARAC divisions (after [30]), and Round Top rhyolite compared with samples from Erzgebirge [29,30], Kymi [28] and chondritic crust.

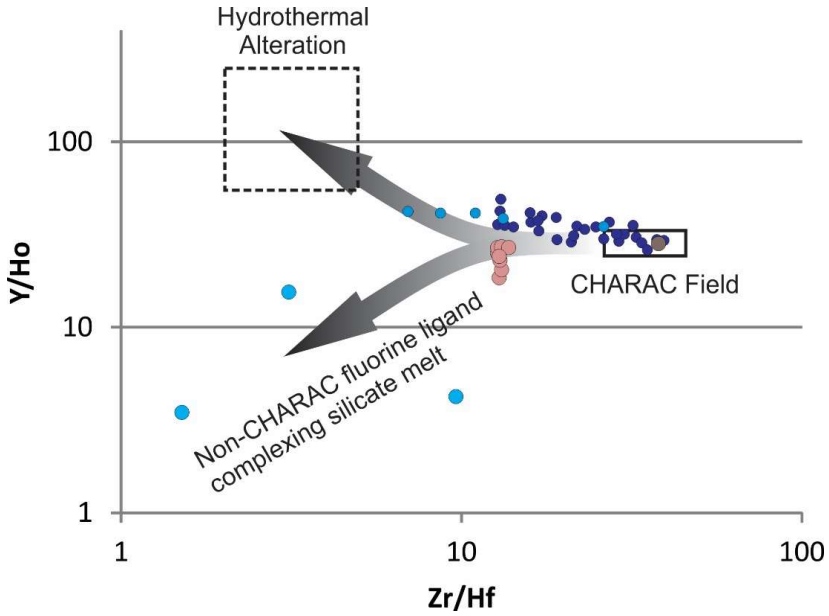

Figure 16. Y/Ho vs. Zr/Hf ratios showing modeled trends toward hydrothermal alteration and non-CHARAC fluorine ligand complexing differentiation with Round Top rhyolite compositions compared with samples from Erzgebirge [29,30], Kymi [28] and chondritic crust. Hydrothermal alteration and CHARAC field(s) adapted from [31]. Symbology the same as Figure 14.

The observed mineral textures trend toward late melt phase REE mineralization in a rapid nucleation environment with a moderate to high degree of undercooling. Geochemical modeling suggests that the Round Top rhyolite HREE enrichment is a result of thorough and long-lived differentiation processes in a fluorine-rich magmatic system, where fluorine complexing with HREE and similar trace elements was pervasive and transitional between low temperature silicate melt and magmatic hydrothermal fluids.

5. Discussion

5.1. Magma Evolution and Emplacement

The conditions and geochemistry necessary to form a rare earth element deposit in highly evolved sub-alkaline rhyolite has not been well documented. The peraluminous composition of Round Top rhyolite differs from peralkaline and metaluminous rhyolites within the TPMP, suggesting a difference in the source material, formation process and/or emplacement timing [3,22,39].

TPMP magmatism and timing of tectonic events were favorable for the formation of continental sourced, highly enriched silicic magma evolving at depth and being emplaced in a shallow environment. The complex tectonic history of the TPMP has had a key role in the development of magmatic source material, providing heat and hosting early mafic to intermediate magmatism. The periodic compressive events punctuated by abrupt stress orientation changes and subsequent extension, overprinted with multiple faulting events and volcanism, created a geologic setting favorable for prolonged isothermal fractionation and differentiation.

The Round Top magma was emplaced in upper Cretaceous fine-grained siliciclastic and carbonate strata, relatively contemporaneous with the formation of the SBC laccoliths, at 36 Ma [6]. Magmatic material that formed the laccolith structure stalled during ascension, extended laterally, and was prevented from erupting at the surface. Rapidly cooled fine-grained groundmass suggests loss of pressure at a higher level in the system, allowing the stalled laccolith magma to quench. The migration of magma through the surrounding Cretaceous country rock was controlled by buoyancy and density contrasts. The nature of the contacts between the laccolith structure, mafic sills and Cretaceous strata suggest the magma was injected along bedding planes at several depths. The rhyolite magma most likely used preexisting magmatic conduits of the diorite sill during emplacement, although enclaves of the preexisting mafic yet to be documented within the rhyolite.

The elevated fluorine content and volatile-rich nature of the magma contributed to the episodic migration of igneous material by altering the viscosity of the magmatic fluids. Elevated fluorine content has been identified as a mechanism for decreasing viscosity of volatile-rich silicic magmas [40,41]. Crystallization of the magma began at depth, and formed phenocrysts of K-feldspar, quartz and plagioclase. Subsequent FC processes continued to differentiate the magma, where isothermal decompression events caused dissolution of K-feldspar and recrystallized as mantle overgrowths on albite phenocrysts. The zoned quartz phenocrysts also provide evidence for prolonged phenocryst residence, where quartz corrosion and re-precipitation (snowball texture) occurred, probably from loss of pressure during multiple minor degassing events. Undercooling textures suggest the groundmass nucleated and crystallized quickly, probably during an eruption event. Interstitial spongy texture in the groundmass and late-stage vapor-phase mineralization in those pore spaces suggests a late- to post-magmatic hydrothermal overprint. The surrounding Cretaceous rock provided an ideal environment to trap residual magmatic fluids, facilitating rapid quenching and crystallization of the groundmass. The rapidly quenching vapor phase formed late-stage trace phases and REE-fluorides. The rhyolite is uniformly, and remarkably, aphanitic and homogenous, suggesting that crystallization of the laccolith as a whole was relatively rapid.

Post-magmatic fluid migrated along fractures and joint surfaces within the rhyolite, oxidizing parts of the laccolith. Fluid-mineral interaction caused magnetite oxidization, forming pervasive hematite alteration. Any color variation in rhyolite is the product of increasing

proportions of hematite and oxidation processes, primarily within the micropores of K-feldspar in the groundmass. Post-magmatic mineralization in the brecciated fractures and joint surfaces is ubiquitous, producing multiple generations of fluorite, calcite and quartz. The pervasive post-magmatic mineralization suggests a prolonged period of remobilization and reprecipitation, facilitated by the circulation of oxidizing, low-temperature, meteoric fluids. The lack of elevated REE concentrations in the surrounding fluoritized limestone and fractures within the rhyolite suggests the post-magmatic conditions were insufficient to remobilize REEs and be incorporated in secondary fluorite.

Disequilibrium textures and the anhedral morphology of groundmass mineralogy throughout the laccolith suggest rapid crystallization. The hourglass sector zonation of the K-feldspar phenocrysts is an unusual disequilibrium texture that occurs as a result of preferential site allocation of sodium and potassium during formation, indicating rapid crystallization and growth during disequilibrium (see Figure 3; [42,43]). Additionally, the pristine outer edge of many of the interior plagioclase laths and interior quartz cores indicate disequilibrium or corrosion of the phenocrysts did not occur until after the formation of overgrowths. The three-part quartz phenocrysts indicate transition from euhedral beta quartz to rapidly crystallizing low-temperature quartz, entraining magmatic melt inclusions. The uniform occurrence of these disequilibrium textures throughout the rhyolite suggests that the change in pressure-temperature conditions affected the entirety of the laccolith, and it is likely that the Round Top laccolith was emplaced as a single magmatic event.

5.2. Timing and Crystallization of REE-Enriched Minerals

The paragenetic sequence of the Round Top mineralogy includes early, middle, and late crystallization phases. These phases were subjected to late-stage alteration from a volatile-rich vapor phase and post-magmatic partial oxidation from circulating fluids. The observed mineralogical relationships between the major, accessory, and trace phases include the formation of early phenocrysts within the magma chamber and continued through emplacement. Albite lathes and the core portions of high-temperature beta quartz phenocrysts formed early. Magma emplacement was relatively rapid, inhibiting significant crystallization during transport as evident by the aphanitic and homogenous nature of the groundmass. As temperature and pressure conditions decreased during emplacement, the subhedral to euhedral, hourglass-type K-feldspar phenocrysts, the K-feldspar overgrowths, the smaller accessory phases, and the larger constituents of the groundmass (K-feldspar, albite, quartz, and annite) began to crystallize. Interaction of these minerals with the circulating high temperature volatile-rich vapor phase produced the dissolution textures observed with the feldspar and quartz populations. During the final stages of crystallization, interaction with the volatile-rich vapor phase produced the alteration textures now observed within the feldspars and quartz overgrowths. Late-stage phases occur interstitial to and within the K-feldspar pores, and include cassiterite, cerianite-(Ce), changbaiite, tantalite, Y- and Ce-rich fluorite, and other nanoscale Y+REE-bearing phases. The intimate association of the REE-fluoride minerals, magnetite, zircon and other trace phases suggests the timing of crystallization was relatively close.

Rubin [7,21] suggested that the early and late zircon populations of the Round Top rhyolite (thorite-rich and thorite-poor) indicate dissolution and recrystallization during subsequent hydrothermal alteration. Selective remobilization of only zircon would require a fluid that could dissolve minerals with relatively immobile geochemical constituents and leave the less robust minerals, such as K-feldspar, plagioclase and quartz, intact. The zircon populations in Round Top rhyolite more likely represent one population with varying degrees of thorite exsolution.

5.3. Heavy Rare Earth Element Enrichment

The Round Top laccolith underwent a pervasive alteration event during late-stage crystallization prior to being oxidized. The alteration event is characterized by partial dissolution and the formation of the "spongy" texture pores spaces within the K-feldspar phenocrysts, overgrowths, and groundmass [44], in addition to forming the undulatory edges in late quartz overgrowths [42].

The strong correlation of REE-minerals to the K-feldspar portion of the rhyolite suggests the availability of open pore space was a significant factor in the retention of the REE-fluoride mineralization. The ubiquitous nature of the quartz embayment and feldspar dissolution suggests the vapor phase alteration was pervasive throughout the entirety of the laccolith, and helps to constrain the timing of REE-bearing mineral precipitation.

The evolution of the Round Top rhyolite and elevated heavy rare earth element concentration requires a suitable chemistry of the protolith and evolving magma that keeps HREEs in the liquid phase until late precipitation at the end of the SBC magmatic evolution. The increased Na, K, and Al in the magma causes increased solubility of rare earths [43]. The fluorine content of the melt is critical to increasing the solubility of REE bearing constituents and keeping the REE in the melt through the evolution of the magma [45,46]. Studies have shown that these compositions can have intermediate properties between silicate melt and hydrothermal fluid allowing for significant amounts of REE- and HFSE-incorporating minerals to crystallize [38,47–50]. Further transport in late-magmatic hydrothermal conditions depends on the availability of ligands in solution that can form stable REE complexes. Although there are environmental considerations and exceptions [51,52], fluorine complexes have been shown to dominate hydrothermal transport of REEs [53,54]. The lack of REE-enrichment in post magmatic fluorite from the surrounding fluoritized limestone suggests that REE mobilization conditions were restricted to late-magmatic to transitional timing.

6. Conclusions

The Round Top rhyolite is enriched in Be, F, Li, Nb, Rb, Sn, Th, U, Y, Zr, and REEs. REE-bearing minerals are mainly ubiquitous nano-scale accessory phases throughout the groundmass, incorporated in synchysite-group minerals, xenotime-(Y), Y-, Ce-, and REE-bearing fluorides, and zircon. The rhyolite is slightly peraluminous, silica-rich, alkaline, with elevated HREE concentrations and a strongly negative Eu-anomaly. Pervasive spongy groundmass and recrystallization textures are consistent with the elevated and remobilized Zr, Th, and Y + HREE concentrations and a HFSE soluble, alkali- and F-rich, magmatic system. REE mineralization is secondary and interstitial, attributed with late-magmatic to transitional vapor-phase mineralization, prior to post-magmatic hydrothermal alteration.

Geochemical modeling provides a better understanding of the geochemical evolution and REE complexing behavior in these rocks, and determines possible source compositions and petrogenetic evolution. The Round Top model suggests an intermediate to mafic crustal protolith or fractionating intermediate to mafic magma could be viable source material. Trace and rare earth element modeling suggests a system typical of having extensive magmatic differentiation, with pulses of emplaced magma represented by the laccoliths of the SBC. The resulting Round Top rhyolite magma is indicative of a high-silica magmatic system rich in H_2O, Li, and/or F transitional between pure silicate melt and hydrothermal fluid, where fluorine-ligand complexing was prevalent through late magmatic cooling and crystallization processes. High fluorine activity and thorough differentiation contributed to the late stage precipitation of REE-bearing minerals in the Round Top rhyolite.

Funding: This research was funded by the Jackson School of Geosciences and the State of Texas Advanced Resource Recovery (STARR) program through the University of Texas at Austin, Bureau of Economic Geology, Mineral Resource Program, and through the United States Geological Survey Mapping Cooperative Program, STATEMAP Award No. G13AC00178.

Acknowledgments: Texas Rare Earth Resources Corporation (now Texas Mineral Resources Corporation) is thanked for permission to conduct research on their property, assistance in conducting fieldwork, and providing access to existing maps, drill hole data, samples, and previous studies. The funding for this study was provided by the Jackson School of Geosciences and the State of Texas Advanced Resource Recovery (STARR) program through the University of Texas at Austin, Bureau of Economic Geology, Mineral Resource Program. This study was greatly enhanced by regional mapping products, produced by the University of Texas at Austin Bureau of Economic Geology, and funded through the United States Geological Survey Mapping Cooperative Program, STATEMAP Award No. G13AC00178. Additional support for student assistants was provided by the III Yager of the Jackson School of Geosciences, the West Texas Geological Society, the Society of Economic Geologists, and

the Association of Environmental and Engineering Geologists. Colleagues, publication editors and anonymous reviewers are thanked for their thoughtful suggestions which greatly improved the manuscript.

Conflicts of Interest: "The authors declare no conflict of interest."

Appendix A

REE and trace element analytical data for Round Top rhyolite and source material derived from regional rocks. K_d values of La in amphibole are from [55], and for other REEs from [56] for dacitic melts. Clinopyroxene values are from [57]. Plagioclase coefficients for La are after [58] and for other REE after [56] for dacitic melts. K-feldspar and biotite coefficients for La from high-silica rhyolites are from [59] and for other REE from [56] for rhyolitic melts. Orthopyroxene data are from [57] for dacite. REE partition coefficient data for basaltic melts are from [57]. Ba and Sr partition coefficients are from [56].

Table A1. Partition coefficients (K_d values) and bulk distribution coefficients (BDC) used in fractional crystallization modeling of regional basaltic andesite (solid lines in Figure 10a) fractionating 40% clinopyroxene (Cpx), 10% hornblende (Hbl), and 50% plagioclase feldspar (Plag).

Element	Cpx	Hbl	Plag	BDC	
Ba	0.0002	0.4200	0.2300	0.1570	
Sr	0.0660	0.4600	1.8300	0.9874	
			Fractionation		
FM-015	ppm	70%	50%	30%	10%
Ba	1299	3584	2330	1755	1420
Sr	1392	1413	1404	1398	1394
FM-013	ppm	70%	50%	30%	10%
Ba	639	640	636	633	631
Sr	660	1791	1164	877	709

Table A2. Partition coefficients (K_d values) and bulk distribution coefficients (BDC) used in melt modeling of regional lithosphere (dotted lines in Figure 10a) fractionating 40% clinopyroxene (Cpx), 10% hornblende (Hbl), 40% plagioclase feldspar (Plag) and 10% alkali feldspar (Kspar).

Element	Cpx	Hbl	Kspar	Plag	BDC		
Ba	0.0002	0.4200	6.1200	0.2300	0.7460		
Sr	0.0660	0.4600	3.8700	1.8300	1.1914		
				% Melt			
PM-52	ppm	5%	10%	30%	50%	70%	90%
Ba	1596	3415	2864	2167	1903	1747	1639
Sr	1230	693	792	977	1077	1149	1205
PM-43	ppm	5%	10%	30%	50%	70%	90%
Ba	685	386	441	544	600	640	671
Sr	736	1575	1321	999	878	806	756

Table A3. Partition coefficients (K_d values) and bulk distribution coefficients (BDC) used in fractional crystallization modeling of early felsic melt (dashed line in Figure 10b) fractionating 3% hornblende (Hbl), 3% biotite (Bt), 57% plagioclase feldspar (Plag), 27% alkali feldspar (Kspar) and 10% quartz (Qtz). Ba and Sr values are in ppm.

Element	Hbl	Bt	Kspar	Plag	Qtz	BDC	
Ba	0.0440	6.3600	6.1200	0.3600	0.022	2.05192	
Sr	0.0220	0.1200	3.8700	2.8400	0.016	2.66956	
				% Fractionation			
	ppm	5%	10%	30%	50%	70%	90%
Ba	2084	1974	1865	1432	1005	587	185
Sr	1006	924	844	555	316	135	22

Table A4. Partition coefficients (K_d values) and bulk distribution coefficients (BDC) used in fractional crystallization modeling of late felsic melt (dotted line in Figure 10b) fractionating 5% biotite (Bt), 75% alkali feldspar (Kspar) and 20% quartz (Qtz). Ba and Sr values are in ppm.

Element	Bt	Kspar	Qtz	BDC			
Ba	6.3600	6.1200	0.022	4.9124			
Sr	0.1200	3.8700	0.016	2.9117			
				% Fractionation			
	ppm	5%	10%	30%	50%	70%	90%
Ba	1432	1171	948	355	95	13	0
Sr	555	503	453	280	147	56	7

Table A5. Partition coefficients (K_d values) used in rare earth element modeling (Figures 11–13).

Element	Cpx	Hbl	Bt	Kspar	Plag	Qtz
La	0.015	0.9	3.18	0.072	0.38	0.015
Ce	0.044	0.899	0.037	0.044	0.24	0.014
Pr	-	-	-	-	-	-
Nd	0.166	2.89	0.044	0.025	0.17	0.016
Sm	0.457	3.99	0.058	0.018	0.13	0.014
Eu	0.411	3.44	0.145	1.13	2.11	0.056
Gd	0.703	5.48	0.082	0.011	0.9	0
Tb	-	-	-	-	-	-
Dy	0.776	6.2	0.097	0.006	0.086	0.017
Ho	-	-	-	-	-	-
Er	0.699	5.94	0.162	0.006	0.084	0.015
Tm	-	-	-	-	-	-
Yb	0.64	4.89	0.179	0.012	0.077	0.017
Lu	0.683	4.53	0.185	0.006	0.062	0.014

Table A6. Bulk distribution coefficients (BDC) and chondrite normalized results (ppm) from fractional crystallization and melting models used in rare earth element modeling (Figures 11–13). Modeled values for Pr, Tb, Ho, and Tm interpolated from Ce and Nd, Gd and Dy, Dy and Er, Er and Yb, respectively.

	Melting of Crustal Granulite (40% cpx, 10% amp, 10% ksp, 40% plag)		Fractionation of Andesitic-Basalt (40% cpx, 10% amp, 50% plag)	
Element	**BDC**	**34%**	**BDC**	**28%**
La	0.2552	110.96	0.2860	85.75
Ce	0.2079	89.63	0.2275	60.69
Pr	-	70.02	-	53.40
Nd	0.4259	50.41	0.4404	46.11
Sm	0.6356	23.93	0.6468	23.05
Eu	1.4654	8.04	1.5634	11.30
Gd	1.1903	21.79	1.2792	20.06
Tb	-	19.10	-	16.33
Dy	0.9654	17.75	0.9734	14.47
Ho	-	16.41	-	12.60
Er	0.9078	15.07	0.9156	10.74
Tm	-	13.72	-	8.87
Yb	0.7770	11.04	0.7835	5.14
Lu	0.7516	11.39	0.7572	9.42

Table A6. *Cont.*

	Fractionation of Early Felsic Assemblage (3 amp, 3% bt, 27% ksp, 57% plag, 10% qtz)			Fractionation of Late Felsic Assemblage (5% bt, 75% ksp, 20% qtz)	
Element	**BDC**	**30%**	**60%**	**BDC**	**30%**
La	0.3599	132.13	189.04	0.2160	140.80
Ce	0.1782	102.70	162.68	0.0377	102.92
Pr	-	85.02	134.22	-	84.51
Nd	0.1933	67.34	105.76	0.0242	66.09
Sm	0.2018	42.20	65.96	0.0192	29.10
Eu	1.6210	21.37	15.10	0.8660	14.27
Gd	0.6828	23.65	28.24	0.0124	29.59
Tb	-	20.62	25.68	-	25.58
Dy	0.2413	18.89	28.88	0.0128	25.79
Ho	-	17.58	23.13	-	21.58
Er	0.2341	13.64	20.94	0.0156	17.36
Tm	-	14.55	20.57	-	17.57
Yb	0.2009	11.52	18.01	0.0214	13.57
Lu	0.1798	12.07	19.10	0.0166	13.59

Appendix B

Table A7. Geochemistry quality control was conducted by blind duplicate analyses, with a known standard(s) and conducted by the commercial analytical facility ACMELABS in Vancouver, B.C., Canada. Major elements and F in weight percent (%), trace and rare earth elements in ppm.

	SiO_2%	Al_2O_3%	Fe_2O_3%	MgO%	CaO%	Na_2O%	K_2O%	TiO_2%
Standard	58.47	14.23	7.67	3.35	6.42	3.71	2.17	0.69
Analysis 1	58.44	14.1	7.48	3.34	6.35	3.58	2.1	0.7
Analysis 2	58.13	14.21	7.59	3.38	6.4	3.57	2.09	0.7
	P_2O_5%	**MnO%**	**Cr_2O_3%**	**FeO%**	**F%**	**Ni**	**Sc**	**Ba**
Standard	0.83	0.39	0.55	15.24	13.4	44	25	514
Analysis 1	0.78	0.4	0.548	15.43	13.09	34	24	517
Analysis 2	0.8	0.4	0.543	-	13.64	33	24	500
	Be	**Co**	**Cs**	**Ga**	**Hf**	**Nb**	**Rb**	**Sn**
Standard	2	26.2	7.1	17.6	9.8	21.3	28.7	15
Analysis 1	3	27.4	6.6	17.5	8.6	18.6	27.6	17
Analysis 2	2	28.7	7.2	16.6	10.2	19.4	29.7	16
	Sr	**Ta**	**Th**	**U**	**V**	**W**	**Zr**	**Y**
Standard	407.4	7.4	9.9	16.4	200	14.8	280	31
Analysis 1	424	6.9	10.1	16.2	216	13.6	300.2	31.8
Analysis 2	445.7	6.6	9.6	17.2	222	16.9	305.3	31.3
	La	**Ce**	**Pr**	**Nd**	**Sm**	**Eu**	**Gd**	**Tb**
Standard	12.3	27.1	3.45	14	3	0.89	2.93	0.53
Analysis 1	13.5	27.3	3.31	13.2	3.07	0.93	2.83	0.44
Analysis 2	13.1	27.8	3.3	14.1	3.15	1	3.08	0.44
	Dy	**Ho**	**Er**	**Tm**	**Yb**	**Lu**		
Standard	3	0.62	1.84	0.27	1.79	0.27		
Analysis 1	3.02	0.66	1.62	0.26	1.81	0.26		
Analysis 2	3.46	0.63	1.97	0.29	2	0.23		
	Mo	**Cu**	**Pb**	**Zn**	**Ni**	**As**	**Cd**	**Sb**
Standard 1	12.84	108	126	317	40.3	25.5	2.4	4.94
Analysis	12.6	116.3	129.1	332	43.2	27.8	2.3	4.7
Standard 2	1.76	709	14.3	30.6	357	11.4	1.03	0.64
Analysis	1.5	720.9	14.6	30	383.4	9.9	<1.0	0.2
	Bi	**Ag**	**Au**	**Hg**	**Ti**	**Se**		
Standard 1	6.32	1.83	118	0.2	5.3	5.2		
Analysis	6.4	1.8	210.6	0.17	4.9	5.6		
Standard 2	0.26	0.311	53	0.34	0.072	2.09		
Analysis	0.2	0.2	54.6	0.02	<1.0	1		

References

1. Pingatore, N.; Clague, J.; Gorski, D. Round top mountain rhyolite (Texas, USA) a massive, unique Y-bearing fluorite-hosted heavy rare earth element (HREE) deposit. *J. Rare Earths* **2014**, *32*, 90–96. [CrossRef]
2. Jowitt, S.M.; Medlin, C.C.; Cas, R.A.F. The rare earth (REE) mineralization potential of highly fractionated rhyolites: A potential low-grade, bulk tonnage source of critical metals. *Ore Geol. Rev.* **2017**, *86*, 549–562. [CrossRef]
3. Price, J.G.; Rubin, J.N.; Henry, C.D.; Pinkston, T.L.; Tweedy, S.W.; Koppenaal, D.W. Rare-metal enriched peraluminous rhyolites in a continental arc, Sierra Blanca area, Trans-Pecos Texas; chemical modification by vapor-phase crystallization. *Geol. Soc. Am. Spec. Pap.* **1990**, *246*, 103–120.
4. Shelley, D. *Igneous and Metamorphic Rocks under the Microscope; Classification, Textures, Microstructures and Mineral Preferred-Orientations*; United Kingdom Chapman & Hall: London, UK, 1992.
5. Barker, D.S. Northern trans-pecos magmatic province: Introduction and comparison with the Kenya rift. *Geol. Soc. Am. Bull.* **1977**, *88*, 1421–1427. [CrossRef]
6. Henry, C.D.; McDowell, F.W. Geochronology of magmatism in the Tertiary volcanic field, Trans-Pecos Texas. In *Bureau of Economic Geology Guidebook*; University of Texas: Austin, TX, USA, 1986; Volume 23, pp. 99–122.
7. Rubin, J.N.; Henry, C.D.; Pinkston, T.L.; Tweedy, S.W.; Koppenaal, D.W. The mobility of zirconium and other "immobile" elements during hydrothermal alteration. *Chem. Geol.* **1993**, *110*, 29–47. [CrossRef]
8. Barker, D.S. Cenozoic magmatism in the Trans-Pecos Magmatic province: Relation to the Rio Grande Rift. In *Rio Grande Rift: Tectonics and Magmatism*; Riecker, R.E., Ed.; Amer Geophys Union: Washington, DC, USA, 1979.
9. Price, J.G.; Henry, C.D.; Barker, D.S.; Parker, D.F. Alkalic rocks of contrasting tectonic settings in Trans-Pecos Texas. *Geol. Soc. Am. Spec. Pap.* **1987**, *215*, 335–346.
10. Henry, C.D.; Price, J.G. Variations in caldera development in the Tertiary volcanic field of Trans-Pecos Texas. *J. Geophys. Res.* **1984**, *89*, 8765–8786. [CrossRef]
11. Barker, D.S. Tertiary alkaline magmatism in Trans-Pecos Texas. *Geol. Soc. Spec. Pub.* **1987**, *30*, 415–431. [CrossRef]
12. Henry, C.D.; Price, J.G.; James, E.W. Mid-Cenozoic stress evolution and magmatism in the southern Cordillera, Texas and Mexico; transition from continental arc to intraplate extension. *J. Geophys. Res.* **1991**, *96*. [CrossRef]
13. Henry, C.D.; Price, J.G.; Miser, D.E. Geology and tertiary igneous activity of the Hen Egg Mountain and Christmas Mountains quadrangles, Big Bend region, Trans-Pecos Texas. In *Bureau of Economic Geology Report of Investigation*; University of Texas: Austin, TX, USA, 1989.
14. Shannon, W.M. Lithogeochemical Characterization of Intrusive Rocks Comprising the Quitman-Sierra Blanca Igneous Complex, Hudspeth County, Texas. Master's Thesis, University of Texas at El Paso, El Paso, TX, USA, 1986.
15. Shannon, W.M.; Goodell, P.C. Lithogeochemistry of intrusive rocks of the Quitman-Sierra Blanca igneous complex, Hudspeth County, Texas. In *University of Texas at Austin Guidebook*; Bureau of Economic Geology: Austin, TX, USA, 1986; Volume 23, pp. 225–236.
16. Dietrich, J.W.; Owen, D.E.; Shelby, C.A.; Barnes, V.E. Geologic Atlas of Texas, map scale 1:250,000. In *Geologic Atlas of Texas, Van Horn-El Paso Sheet*; The University of Texas at Austin, Bureau of Economic Geology: Austin, TX, USA, 1983.
17. Albritton, C.C., Jr.; Smith, J.F., Jr. *Geology of the Sierra Blanca Area, Hudspeth County, Texas*; The United States Geological Survey: Reston, VA, USA, 1965; pp. 1044–9612.
18. Henry, C.D.; McDowell, F.W.; Price, J.G.; Smyth, R.C. Compilation of potassium-argon ages of Tertiary igneous rocks, Trans-Pecos Texas. In *Geological Circular 86-2*; The University of Texas at Austin, Bureau of Economic Geology: Austin, TX, USA, 1986; p. 34.
19. Matthews, W.K., III; Adams, J.A.S. Geochemistry, age, and structure of the Sierra Blanca and Finlay Mountain intrusions, Hudspeth County, Texas. In *Bureau of Economic Geology, University of Texas at Austin Guidebook*; The University of Texas at Austin, Bureau of Economic Geology: Austin, TX, USA, 1986; Volume 23, pp. 207–224.
20. Rubin, J.N.; Price, J.G.; Henry, C.D.; Kyle, J.R. Geology of the beryllium-rare earth element deposits at Sierra Blanca, West Texas. *Soc. Econ. Geol. Guideb. Ser.* **1990**, *8*, 191–203.

21. Rubin, J.N.; Henry, C.D.; Price, J.G. Hydrothermal zircons and zircon overgrowths, Sierra Blanca Peaks, Texas. *Am. Mineral.* **1989**, *74*, 865–869.
22. Rubin, J.N.; Price, J.G.; Henry, C.D.; Koppenaal, D.W. Cryolite-bearing and rare metal-enriched rhyolite, Sierra Blanca Peaks, Hudspeth County, Texas. *Am. Mineral.* **1987**, *72*, 1122–1130.
23. O'Neill, L.C. REE–Be–U–F mineralization of the Round Top Laccolith, Sierra Blanca Peaks, Trans-Pecos Texas. Master's Thesis, University of Texas at Austin, 2013; p. 209.
24. Li, Y.; Barnes, M.A.; Barnes, C.G.; Frost, C.D. Grenville-age A-type and related magmatism in southern Laurentia, Texas and New Mexico, U.S.A. *Lithos* **2007**, *97*, 58–87. [CrossRef]
25. Morris, P.A. MAGFRAC: A basic program for least-squares approximation of fractioanl crystallization. *Comput. Geosci.* **1984**, *10*, 437–444. [CrossRef]
26. Pearce, J.A.; Niger, B.W.H.; Tindle, G. Trace element discrimination diagrams for the tectonic interpretation of granitic rocks. *J. Petrol.* **1984**, *24*, 956–983. [CrossRef]
27. Boynton, W. Cosmochemistry of the rare earth elements: Meteorite studies. In *Rearth Element Geochemistry*; Henderson, P., Ed.; Elsevier Sci Publ Co.: Amsterdam, The Netherlands, 1984; pp. 63–114.
28. Haapala, I.; Lukkari, S. Petrological and geochemical evolution of the Kymi stock, a topaz granite cupola within the Wiborg rapakivi batholith, Finland. *Lithos* **2004**, *80*, 347–362. [CrossRef]
29. Irber, W.; Förster, H.J.; Hecht, L.; Miller, P.; Morteani, G. Experimental, geochemical, mineralogical and O-isotope constraints on the late-magmatic history of the Fichtelgebirge granites (Germany). *Geol. Rund.* **1997**, *86*, 110–124. [CrossRef]
30. Irber, W. The lanthanide terad effect and its correlation with K/Rb, Eu/Eu*, Sr/Eu, Y/Ho, and Zr/Hf evolving peraluminous granite suites. *Geochim. Cosmochim. Acta* **1999**, *63*, 489–508. [CrossRef]
31. Bau, M. Controls on the fractionation of isovalent trace elements in magmatic and aqueous systems: Evidence from Y/Ho, Zr, Hf, and lanthanide tetrad effect. *Contrib. Mineral. Petrol.* **1996**, *123*, 232–333. [CrossRef]
32. Kawabe, I. Lanthanide tetrad effect in the Ln^{3+} ionic radii and refined spin-pairing energy theory. *Geochem. J.* **1992**, *26*, 309–335. [CrossRef]
33. Monecke, T.; Kempe, U.; Monecke, J.; Sala, M.; Wolf, D. Tetrad effect in rare earth element distribution patterns: A method of quantification with application to rock and mineral samples from granite-related rare metal deposits. *Geochim. Cosmochim. Acta* **2002**, *66*, 1185–1196. [CrossRef]
34. Van Lichtervelde, M.; Grand'Homme, A.; de Saint-Blanquat, M.; Olivier, P.; Gerdes, A.; Paquette, J.L.; Melgarejo, J.; Druguet, E.; Alfonso, P. U-Pb geochronology on zircon and columbite-group minerals of the Cap de Creus pegmatites, NE Spain. *Mineral. Petrol.* **2017**, *111*, 1–21. [CrossRef]
35. Peretyazhko, J.S.; Savina, E.A. Tetrad effects in rare earth element patterns of granitoid rocks as an indicator of fluoride–silicate liquid immiscibility in magmatic systems. *Petrology* **2010**, *18*, 536–566. [CrossRef]
36. Thomas, R.; Förster, H.; Rickers, K.; Webster, J.D. Formation of extremely rich F-rich hydrous melt fractions and hydrothermal fluids during differentiation of highly evolved tin-granite magmas: A melt/fluid-inclusion study. *Contrib. Mineral. Petrol.* **2005**, *148*, 582–601. [CrossRef]
37. Agangi, A.; Kamanetsky, V.S.; McPhie, J. The role of fluorine in the concentration and transport of lithophile trace elements in felsic magmas: Insights from the Gawler Range volcanics, South Australia. *Chem. Geol.* **2010**, *273*, 314–325. [CrossRef]
38. Thomas, R.; Davidson, P.; Beurlen, H. The competing models for the origin and internal evolution of granitic pegmatites in the light of melt and fluid inclusion research. *Mineral. Petrol.* **2012**, *106*, 55–73. [CrossRef]
39. Barker, D.S. Cenozoic igneous rocks, Sierra Blanca area, Texas. In *New Mexico Geological Society Guidebook 31st Field Conference*; Dickerson, P.W., Hoffer, J.M., Callender, J.F., Eds.; New Mexico Geological Society: Socorro, NM, USA, 1980; pp. 219–223.
40. Giordano, D.; Romano, C.; Dingwell, D.B.; Poe, B.; Behrens, H. The combined effects of water and fluorine on the viscosity of silicic magmas. *Geochim. Cosmochim. Acta* **2004**, *68*, 5159–5168. [CrossRef]
41. Vernon, R.H. *A Practical Guide to Rock Microstructure*; Cambridge University Press: Cambridge, UK, 2004.
42. O'Neill, L.C.; Elliott, B.A.; Kyle, J.R. Mineralogy and crystallization history of a highly differentiated REE-enriched hypabyssal rhyolite: Round Top laccolith, Trans-Pecos, Texas. *Mineral. Petrol.* **2017**, *111*, 569–592. [CrossRef]
43. Watson, E.B. Zircon saturation in felsic liquids: Experimental results and applications to trace element geochemistry. *Contrib. Mineral. Petrol.* **1979**, *70*, 407–419. [CrossRef]

44. Negron, L.; Pingatore, N.; Gorski, D. Porosity and permeability of Round Top mountain rhyolite (Texas, USA) favor coarse crush size for rare earth element heap leach. *Minerals* **2016**, *6*, 1–16. [CrossRef]
45. Keppler, H. Influence of fluorine on the enrichment of high field strength trace elements in granitic rocks. *Contrib. Mineral. Petrol.* **1993**, *114*, 479–488. [CrossRef]
46. Farges, F. Does Zr–F 'complexation' occur in magmas? *Contrib. Mineral. Petrol.* **1996**, *127*, 253–268. [CrossRef]
47. London, D.; Hervig, R.L.; Morgan, G.B. VI Melt-vapor solubilities and elemental partitioning in peraluminous granite–pegmatite systems: Experimental results with Macusani glass at 200 MPa. *Contrib. Mineral. Petrol.* **1988**, *99*, 360–373. [CrossRef]
48. Webster, J.D. Partitioning of F between $H_2O \pm CO_2$ fluids and topaz rhyolite melt: Implications for mineralizing magmatic-hydrothermal fluids in F-rich granitic systems. *Contrib. Mineral. Petrol.* **1990**, *104*, 424–438. [CrossRef]
49. Thomas, R.; Davidson, P.; Rhede, D.; Leh, M. The miarolitic pegmatites from the Konigshain: A contribution to understanding the genesis of pegmatites. *Contrib. Mineral. Petrol.* **2009**, *157*, 505–523. [CrossRef]
50. Keppler, H.; Wyllie, P.J. Role of fluids in transport and fractionation of uranium and thorium in magmatic processes. *Nature* **1990**, *348*, 531–533. [CrossRef]
51. Migdisov, A.A.; Williams-Jones, A.E.; Wagner, T. An experimental study of the solubility and speciation of the rare earth elements (III) in fluoride- and chloride-bearing aqueous solutions at temperatures up to 300 °C. *Geochim. Cosmochim. Acta* **2009**, *73*, 7087–7109. [CrossRef]
52. Migdisov, A.A.; Williams-Jones, A.E. An experimental study of the solubility and speciation of neodymium (III) fluoride in F-bearing aqueous solutions. *Geochim. Cosmochim. Acta* **2007**, *71*, 3056–3069. [CrossRef]
53. Samson, I.M.; Kerr, I.D.; Graf, C. The rock canyon creek fluorite—REE deposit, British Columbia. In *Industrial Minerals in Canada*; Dunlop, S., Simandl, G.J., Eds.; Canadian Institute of Mining, Metallurgy and Petroleum Special: Westmount, QO, Canada, 2001; Volume 53, pp. 35–44.
54. Williams-Jones, A.E.; Samson, I.M.; Olivo, G.R. The genesis of hydrothermal fluorite-REE deposits in the Gallinas Mountains, New Mexico. *Econ. Geol.* **2000**, *95*, 327–341. [CrossRef]
55. Henderson, P. *Rare Earth Element Geochemistry*; Elsevier: Amsterdam, The Netherlands, 1984.
56. Arth, J.G. Behavior of trace elements during magmatic processes: A summary of theoretical models and their applications. *J. Res. U.S. Geol. Surv.* **1976**, *4*, 41–47.
57. Fujimaki, H.; Tatsumoto, M.; Aoki, K. Partition coefficients of Hf, Zr, and REE between phenocrysts and groundmasses. *J. Geophys. Res.* **1984**, *89*, B662–B672. [CrossRef]
58. Nash, W.P.; Crecraft, H.R. Partition coefficients for trace elements in silicic magmas. *Geochim. Cosmochim. Acta* **1985**, *49*, 2309–2322. [CrossRef]
59. Mahood, G.A.; Hildreth, E.W. Large partition coefficients for trace elements in high-silica rhyolites. *Geochim. Cosmochim. Acta* **1988**, *47*, 11–30. [CrossRef]